Materials Advances

ROYAL SOCIETY OF CHEMISTRY

PAPER

View Article Online
View Journal

Cite this: DOI: 10.1039/d6ma00171h

Large-scale tubular protonic ceramic electrolysis cells made by injection molding

You-Dong Kim,[a] Javishk Shah,[b] Christopher Schiller,[c] Ryan O'Hayre [a] and Sandrine Ricote *[bd]

Received 6th February 2026,
Accepted 27th May 2026

DOI: 10.1039/d6ma00171h

rsc.li/materials-advances

Protonic ceramic electrochemical cells (PCCs) are potential candidates for efficient hydrogen production at intermediate temperature (~400–600 °C). However, their development has been limited to the laboratory scale. Here, we report the first demonstration of large-scale tubular PCCs *via* ceramic injection molding. NiO-$BaCe_{0.7}Zr_{0.1}Y_{0.1}Yb_{0.1}O_{3-d}$ (BCZYYb7111) closed-end negatrode supports are injection-molded into uniform, straight tubes with a diameter of 1.5 cm and lengths up to 17.5 cm; the BCZYYb7111 electrolyte is then dip-coated and co-sintered. Microstructural analysis confirms homogeneous phase distribution, well-controlled porosity in the reduced negatrode, and a high-quality, dense, and crack-free electrolyte with exceptionally large grain size (~50 μm) and thicknesses between 24 and 30 μm. Under electrolysis operation, these tubes achieve current densities up to 400 mA cm^{-2} at 1.3 V and 650 °C. Stable operation for 50 hours at 250 mA cm^{-2} and 550 °C is also demonstrated.

1. Introduction

Protonic ceramic electrochemical cells (PCCs) are promising technology for reversible energy storage and green hydrogen production at intermediate temperatures (~400–600 °C).[1–4] This temperature range allows for reduced stack material costs, high flexibility for material selection, and potentially improved stability compared to high-temperature solid oxide fuel cells.[5] For hydrogen production, lowering operating temperatures enables a total hydrogen production cost reduction. Additionally, PCCs produce nominally dry hydrogen that is directly amenable to electrochemical compression.

Despite those advantages, PCCs are new technology with a technology readiness level (TRL) of about 4, *i.e.* component-level validation in a laboratory environment.[6] Further achievements are essential to develop commercially viable PCC devices capable of facilitating cost-effective hydrogen production. Beyond laboratory-scale devices, the development of large-scale PCCs *via* mass-production capable processes should be prioritized to achieve commercialization.

When solid oxide electrochemical devices pursued large-scale levels, other parts (sealant, bipolar plate, current collector, *e.g.*) were also considered to inform stack-level scale-up requirements.[7] Tubular configurations can offer advantages compared to the planar geometry, thereby reducing stack complexity.[8,9] Tubular PCCs have inherent geometric benefits such as thermal shock resistance, compressive strength, and minimization of sealing requirements. In some cases, it is possible to extend tubes out of the hot zone, which makes sealing somewhat less difficult.

Several approaches have been explored to fabricate large-scale tubular devices, such as slip casting, extrusion, phase inversion, *etc.*[8,10,11] Ceramic processing for tubular PCCs frequently requires non-aqueous solvents, which involve toxic byproducts and hazardous additives.[12,13] Injection molding is an established, scalable technique that can form functional ceramic components with complex shapes.[14,15] It enables quick processing, low cost, and high yield. In a typical injection molding process, powder is combined with an optimized binder and injected into a mold, where the green body is formed under high pressure and temperature conditions (300–800 bar, and 120–200 °C).[16] Green-body injection-molded tubes have high mechanical strength and are easy to handle without any post-drying process. Unlike other tubular ceramic processing techniques, injection molding exhibits lower material losses, thereby decreasing the overall cost.[17–20] This technique has previously been exploited in the solid oxide fuel cell (SOFC) field. Jardiel *et al.* first applied injection molding to SOFCs.[17] Jakub *et al.* investigated Ni-YSZ anode-supported SOFC using high-pressure injection molding.[21] Although the potential of injection molding has therefore been established for SOFCs, it has not yet been reported for PCCs.

[a] *Department of Metallurgical and Materials Engineering, Colorado Center for Advanced Ceramics, Colorado School of Mines, Golden, CO 80401, USA. E-mail: sricote@mines.edu*
[b] *HyET NoCarbon, Golden, CO 80401, USA. E-mail: sandrine.ricote@hyetnocarbon.com*
[c] *Allied Tech Supply (ATS), Alpharetta, GA 30004, USA*
[d] *Department of Mechanical Engineering, Colorado School of Mines, Golden, CO 80401, USA*

In this study, we demonstrate the potential of injection molding for large-scale closed-end tubular PCC production. NiO-$BaCe_{0.7}Zr_{0.1}Y_{0.1}Yb_{0.1}O_{3-d}$ (BCZYYb7111) negatrodes were shaped into uniform and straight tubes *via* the injection molding process. The BCZYYb7111 electrolyte was then dip-coated and co-sintered to form crack-free and dense electrolytes. We observe well-distributed Ni (upon reduction) and BCZYYb7111 phases *via* scanning electron microscopy. The electrolyte thickness is quite homogeneous across the length of the tube. A newly developed high-entropy perovskite oxide was adapted as the air-steam (*i.e.*, positrode) electrode for large-scale (20 cm^2 active area) injection molded tubular PCCs. We achieved 400 mA cm^{-2} under electrolysis operating conditions at 1.3 V.

2. Experimental

The injection-molded tubes were prepared using a 40/60 composite of BCZYYb7111 and NiO powders. The BCZYYb7111 powder was from Cerpotech (lot# 290912A-BCZYYb7111), and the NiO powder from Novamet (green NiO type F, product number 201-891-7976, lot # 20705). The powder composite (40/60 BCZYYb7111/NiO) was ball milled with zirconia media in acetone for 26 hours. ATS developed a proprietary binder system suitable to injection molding 7″ long × 0.6″ diameter tubes using this powder composition. The feedstock was designed with high solid loadings (around 60%), primary (around 25%) and secondary (around 10%) binders (for flow and green strength functions, respectively) as well as dispersants (<5%) and was mixed in a small production mixer. The feedstock is formulated to be shear thinning, *i.e.* a lowered viscosity is obtained at high shear forces. The tubes were molded on a small production PIM injection molding machine. While the mold temperature remains below 80 °C, the injection temperature was adjusted between 150 and 200 °C, with molding pressures between 100 and 200 MPa. To avoid defects in the molded tubes, the injection speed was kept below 30 cm^2 s^{-1}. Once the feedstock formulation and molding parameters were optimized, high yields above 90% could be obtained. The tubes were visually examined for cracks or defects, and for concentricity. After molding, the full-length tubes were debound in air at 310 °C. Then, they were bisque-fired at 1030 °C in air.

The BCZYYb7111 electrolyte was dip-coated on the bisque-fired NiO-BCZYYb7111 supports using a dip-coater that was custom fabricated in-house using aluminum framing and a motor-actuated linear rail. A custom fixture was designed to secure the tube to the linear rail, and the tube was interfaced to the fixture using an Ultra-Torr fitting from Swagelok. Operation of the linear rail was controlled through automated software. Multiple dry runs were performed to verify the safe operation of the system and to protect the tube. The ethanol-based dip-coating electrolyte slurry used the same Cerpotech BCZYYb7111 powder that was used in the support. PVP was selected as a binder and dispersant. The tubes were coated twice for 1 second with a 10-minute drying time in between. The tubes were afterwards hang-fired. Holes were drilled on the upper part of the tubes (away from the tip) and an alumina rod was used to hold the tube. After a debindering step at 450 °C, the tubes were sintered 6 hours at 1500 °C. The dimensions of the sintered parts are: diameter about 0.5 inches and length between 5 and 6 inches, leading to active areas of at least 40 cm^2. Fig. S1 shows the tubes with the hanging rods after sintering.

The $Ba_{0.9}Cs_{0.1}(Ca_{0.2}Gd_{0.2}La_{0.2}Pr_{0.2}Sr_{0.2})Co_{1.5}Fe_{0.5}O_{6-d}$ high-entropy positrode (CsBaHEO) was synthesized *via* the EDTA-citric acid complexing sol–gel route.[22] Stoichiometric amounts of $Ba(NO_3)_2$ (Alfa Aesar, 99%), $Cs(NO_3)$ (Alfa Aesar, 99%), $La(NO_3)_3$ $6H_2O$ (Alfa Aesar, 99.9%), $Sr(NO_3)_2$ (Alfa Aesar, 99%), $Pr(NO_3)_3$ $6H_2O$ (Alfa Aesar, 99%), $Gd(NO_3)_3$ $6H_2O$ (Alfa Aesar, 99%) $Co(NO_3)_2$ $6H_2O$ (Alfa Aesar, 98–102%), $Fe(NO_3)_2$ $9H_2O$ (Alfa Aesar, 98%), in dilute nitric acid (Sigma Aldrich) and $Y(NO_3)_3$ $6H_2O$ (Alfa Aesar, 99.9%) were stirred in deionized water, with ethylenediaminetetraacetic acid (EDTA) and citric acid. The molar ratio of EDTA : citric acid : total metal ions was 1.5 : 1.5 : 1. Subsequently, ammonium hydroxide (NH_3 H_2O) was added to adjust the pH value to around 9, and heated on a hot plate at 280 °C. Once a dark purple gel was formed, it was placed in a drying oven (Thermo Fisher Scientific, UNK) at 150 °C for 24 h. The resulting black charcoal was crushed with a mortar and pestle, then pre-calcined at 600 °C for 5 h, followed by ball milling with isopropanol (IPA) and 3 mm yttria-stabilized zirconia (YSZ) balls for 24 h. The powder was then dried in a heating oven at 90 °C. To improve the positrode adhesion properties, pre-calcined air/steam electrode powder (600 °C) was used. It was mixed with 5 wt.% V-006A in alpha terpineol, and 20 wt. % Solsperse 28 000 in alpha terpineol as dispersant to make the positrode paste. The paste was brush-painted on top of the electrolyte; the active area of the positrode was 20 cm^2. It was not possible to use the entire tube for electrochemical testing due to test stand limitations; the tested 20 cm^2 active area section represents only a portion of one tube. The complete cell was fired at 900 °C for 5 h with heating and cooling rates of 2 °C min^{-1}.

Pt paste was applied on top of the positrode, and then silver grids were brush-painted. Silver wire was wrapped around the positrode. For the negatrode current collection, Ni powder (Fisher scientific, 99.9%) was mixed with binder (Heraeus V006) to form a paste that was subsequently applied inside the tube (as current collector) using a thin pipe cleaner. After that, silver wire was placed on fuel electrode side. The tubes were baked for an hour on a hot plate at 200 °C to cure all pastes.

Tubular PCCs were mounted on alumina feed tubes (CoorsTek) using ceramic adhesive (Ceramabond 552-VFG) and secured within a custom-designed tubular test stand, including high-temperature clamshell furnace (ATS), for electrochemical-performance testing. For electrolysis mode, the cells were operated under dry H_2 at the negatrode (100 ml min^{-1}) and humidified synthetic air (30 vol% H_2O, 600 ml min^{-1}) at the positrode electrode. Air passed through heated lab-made bubbler with Nafion tube (Perma Pure) to facilitate complete water saturation of the air. Durability testing was conducted under

Fig. 1 Bisque-fired 7-inch-long injection molded NiO-BCZYYb7111 tubes.

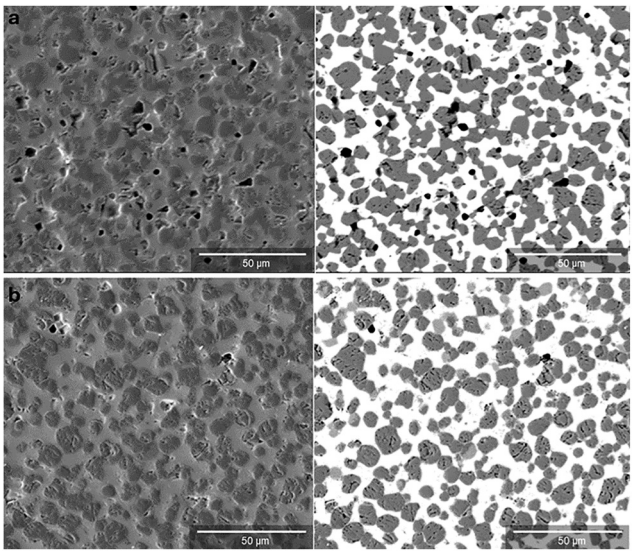

Fig. 2 (a) Micrographs of polished NiO-BCZYYb cross section. An injection-molded tube was sintered at 1500 °C without electrolyte. (b) Micrographs of polished Ni-BCZYYb. This cross section is from the same tube as in Fig. 2a, but after reduction: 24 hours at 600 °C in 3% H_2/argon. Left: Secondary electrons – Right: Backscattered electrons.

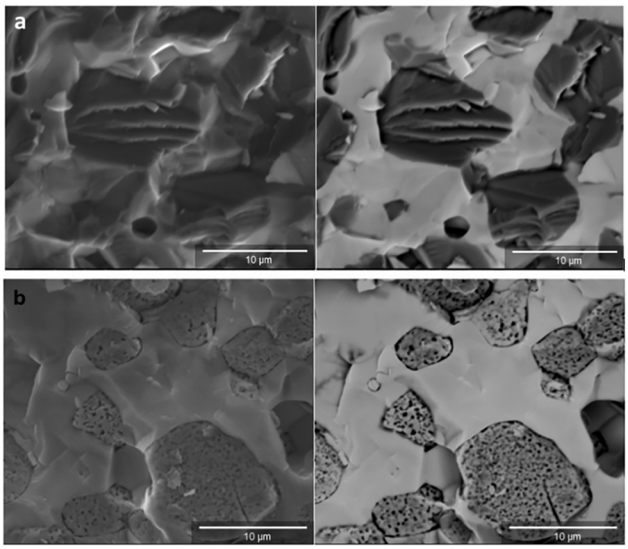

Fig. 3 Micrographs of fractured (a) NiO-BCZYYb and (b) Ni-BCZYYb-Ni. Left: Secondary electrons – Right: Backscattered electrons.

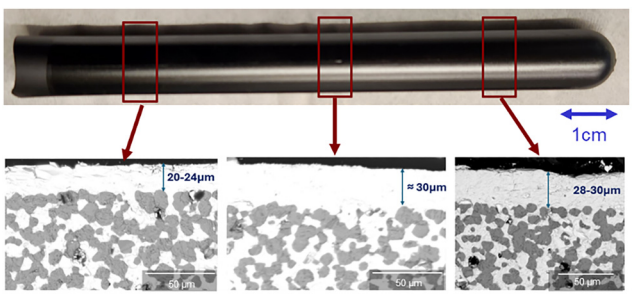

Fig. 4 Evolution of the sintered BCZYYb7111 electrolyte thickness along the tube.

galvanostatic mode with 250 mA cm^{-2}. Polarization scans were measured using a power supply (B&K precision) due to the high currents. Electrochemical impedance spectroscopy (EIS) was performed using a Gamry Reference 5000 potentiostat. The EIS measurements were performed at open circuit voltage using a signal amplitude of 10 mV in the frequency range of 10^6 to 0.1 Hz.

Scanning electron micrographs were collected on fractured cross sections of a bisque-fired tube as well as a bisque-fired tube after the dip coating process (and before sintering) using a FEI Quanta 600I Environmental Scanning Electron Microscope (ESEM). A support tube (NiO-BCZYYb7111) was sintered without an electrolyte to study its morphology. Polished and fractured cross sections were studied using a FEI Quanta 600I ESEM. Part of this tube was also reduced (24 hours at 600 °C, in 3% H_2/argon) and its microstructure was studied as well. Additionally, three cross sections of a sintered NiO-BCZYYb7111//BCZYYb7111 tube were cut at different locations, one at the top, one in the middle and one towards the bottom of the tube. The cross sections were set in epoxy and polished. After gold coating, secondary and back-scattered micrographs were collected (FEI Quanta 600I ESEM) to determine the thickness variation along the length of the tubes. Micrographs of the surface of the electrolyte were also taken. Lastly, cross-micrographs were also collected on the complete NiO-BCZYYb7111//BCZYYb7111//CsBaHEO cells, using an FEI Nova NanoSEM. Micrographs were collected on a tube both before and after testing.

3. Results and discussion

Examples of injection molded tubes before and after bisque-firing are shown in Fig. S2 and Fig. 1, respectively. Circular, strong, high-quality, and reproducible 7-inch-long closed-end tubes with excellent surface finish are obtained.

Fig. 2a and b display the micrographs of polished cross-sections of the NiO-BCZYYb and Ni-BCZYYb supports, respectively.

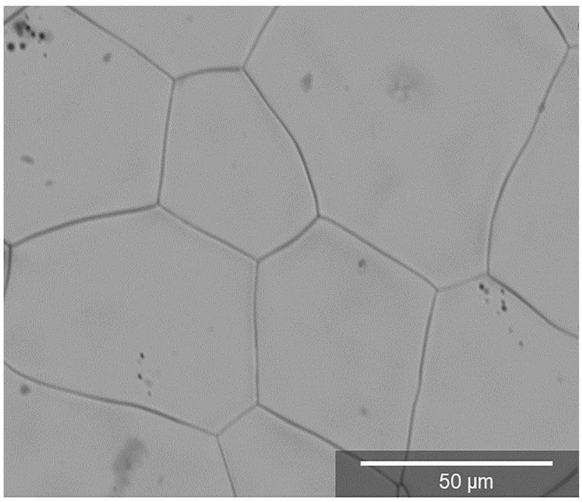

Fig. 5 SEM of the surface of the sintered BCZYYb7111 electrolyte.

The left image (from SE, or secondary electron imaging mode), provides information on the microstructure, while the right image (from BSE, or backscattered electron imaging mode) accentuates contrast due to composition ("z-contrast"). The phase containing higher-z elements (BCZYYb) is white in the BSE image, while the NiO/Ni phase is grey. From the polished cross-section images, a few pores can be observed. The NiO/Ni grains are 3 to 10 microns, but the average grain size within the BCZYYb phase could not be estimated.

Fig. 3a and b exemplify the micrographs of the fractured cross-sections of the NiO-BCZYYb and Ni-BCZYYb samples, respectively (same tube as for Fig. 2a and b but not polished). The NiO grains exhibit a platelike microstructure, which explains the porosity observed in the polished cross-sections. Upon reduction, the nickel grains present the expected porous sponge-like microstructure.

Fig. S3 and S4 display scanning electron micrographs of the bisque-fired tube and of the dip-coated tube before sintering. The bisque-fired NiO-BCZYYb support presents porosity (from the organics burn out) and submicron NiO and BCZYYb grains. It is interesting to note that the dip-coated BCZYYb layer does not penetrate the support. The average thickness of the dip-coated layer before sintering is 30 microns.

In the top part of Fig. 4, a full-length sintered tube is pictured. The shrinkage upon sintering is about 17%. The three locations where cross-sections were cut are indicated with the red boxes. The corresponding micrographs are shown below, with the electrolyte thickness varying from 24 microns at the top of the tube to 30 microns towards the closed end of the

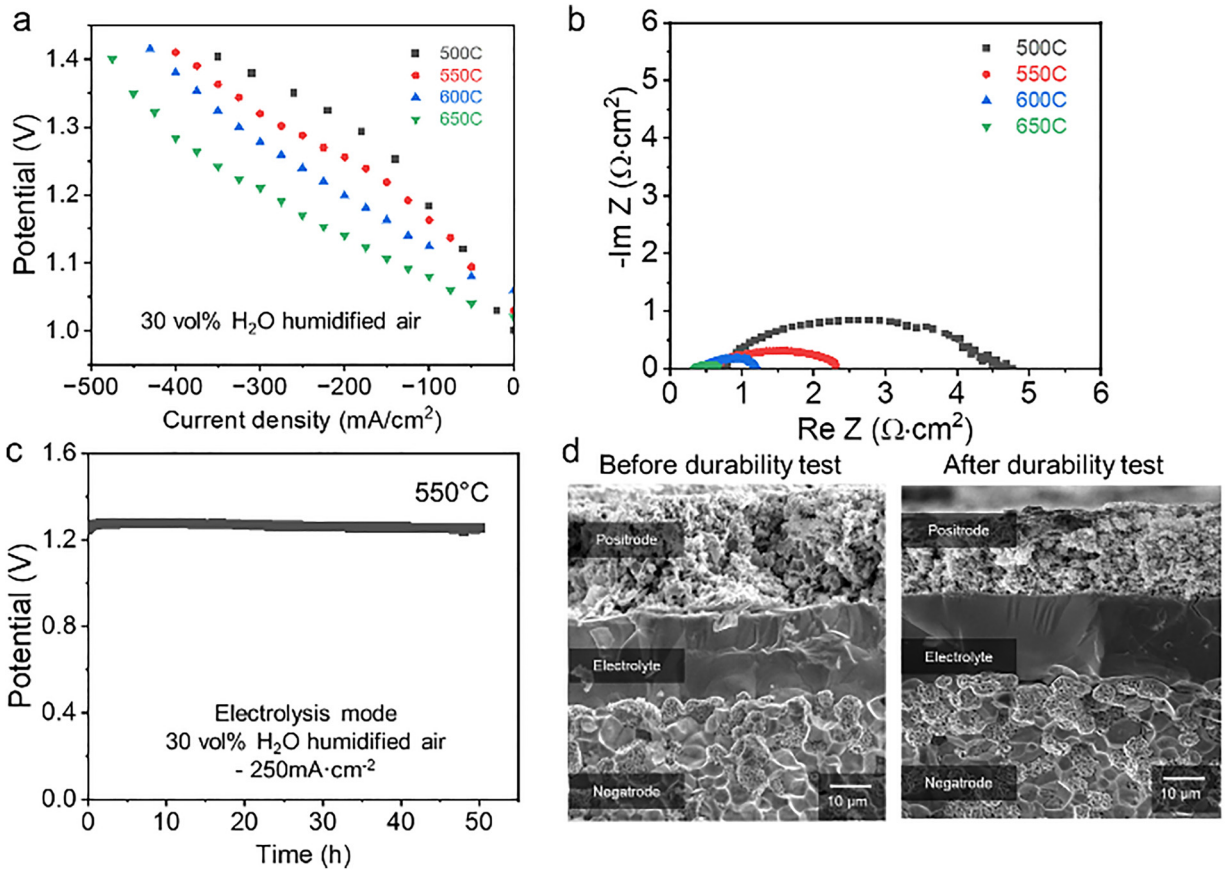

Fig. 6 (a) Current density and potential curve under 30 vol% humidified air the temperature range from 500 to 650 °C. (b) Nyquist plot at various temperatures. (c) Durability test under electrolysis mode at −250 mA cm^{-2} and 550 °C. (d) Cross-sectional SEM image of negatrode/electrolyte/positrode of large-scale tubular PCC before and after durability testing.

tube. Such variations are expected as the closed-end part of the tube stays longer in the dip-coating slurry. This thickness variation is within the acceptable range. Additionally, the reproducibility of this dip-coating process was confirmed as the thickness of the dip-coated layer on several tubes was in the same range: 24 to 31 microns (Fig. S5).

The surface of the electrolyte, Fig. 5, confirms that a well-sintered membrane with large grains (around 50 microns) was obtained after co-sintering the electrolyte onto the bisque-fired injection molded tubes.

The injection molded tube was tested in electrolysis mode under 30 vol% of humidified synthetic air at the positrode and hydrogen at the negatrode. The *I–V* performance and electrochemical impedance spectroscopy (EIS) under OCV were evaluated at temperatures ranging from 500 to 650 °C (Fig. 6a and b). Current densities of 180, 275, 325, and 400 mA cm^{-2} were obtained at thermoneutral voltage at 500, 550, 600, and 650 °C, respectively. OCV values above 1 V across the tested temperature range confirm the gas-tightness of the electrolyte.

The ohmic resistance (electrolyte and contact resistances) and polarization resistances (related to the electrodes) can be extracted from the Nyquist plots in Fig. 6b. Ohmic resistances are 0.77, 0.63, 0.46, and 0.35 Ω cm^2 and polarization resistances are 4.08, 1.68, 0.74, and 0.31 Ω cm^2 at 500, 550, 600, and 650 °C, respectively. As expected, both resistances decrease with increasing temperature. An example of DRT for the spectrum collected at 600 °C is given in Fig. S6, highlighting the higher contribution of the positrode (low frequency) to the total polarization resistance compared to the negatrode (high frequency).

Short-term durability testing under electrolysis mode was conducted at 550 °C. Under galvanostatic operation at 250 mA cm^{-2}, the cell potential increases by 0.002 V (0.16%) from 1.251 to 1.253 V over 50 hours. EIS spectra before and after testing are shown in Fig. S7, together with the corresponding DRTs: the major polarization increase happens at low frequencies, corresponding to what is generally associated to be positrode-related contributions to the polarization resistance. A potential explanation for these positrode-focused degradation losses could be electrochemically-driven microstructural evolution processes (*e.g.* such as agglomeration) within the positrode.[23]

The cross-sectional SEM of the complete cell before *vs.* after testing is shown Fig. 6d, with the dense electrolyte sandwiched between the porous Ni-BCZYYb negatrode (sponge-like microstructure) and the high-entropy double perovskite oxide porous positrode.

4. Conclusions

Large-scale closed-end tubular PCCs were successfully fabricated using injection molded closed-end tubular supports, demonstrating a scalable manufacturing route for PCCs. NiO-BCZYYb7111 negatrode supports were formed by injection molding. A uniform electrolyte layer (BCZYYb7111) was dip-coated on the large-scale negatrode supports and co-sintered, resulting in a highly dense electrolyte film with exceptionally large grain size (~50 μm). Microstructural analysis demonstrated a well-distributed co-percolating phase network with interconnected porous Ni particles after reduction. Additionally, the electrolyte thickness was observed to vary between 24 and 30 microns, attributed to differences in the exposure time to the dip-coating solution along the length of the tube. High-entropy double perovskite oxide ($Ba_{0.9}Cs_{0.1}(Ca_{0.2}Gd_{0.2}La_{0.2}Pr_{0.2}Sr_{0.2})Co_{1.5}Fe_{0.5}O_{6-d}$ (CsBaHEO)) was applied as positrode over a 20 cm^2 active area. The tubular PCC yielded an electrolysis current density of 400 mA cm^{-2} at 1.3 V and 650 °C. Stable operation at 250 mA cm^{-2} for 50 hours further demonstrates the potential of this approach. These results, the first for injection-molded PCC tubes, confirm that injection molding is a promising pathway toward scalable, high-performance PCC devices. Further development will focus on decreasing electrolyte thickness and testing different positrode materials.

Author contributions

Youdong Kim: conceptualization, validation, formal analysis, investigation, data curation, writing – original draft, writing – review & editing. Javishk Shah: conceptualization, writing – review & editing. Christopher Schiller investigation, formal analysis. Ryan O'Hayre: writing – review & editing. Sandrine Ricote: conceptualization, validation, formal analysis, funding acquisition, investigation, data curation, writing – original draft, writing – review & editing.

Conflicts of interest

There are no conflicts to declare.

Data availability

The BCZYYb-NiO//BCZYYb half cells were prepared by a novel combination of dip coating the electrolyte onto injection molded supports.

The high entropy positrode material ($Ba_{0.9}Cs_{0.1}(Ca_{0.2}Gd_{0.2}La_{0.2}Pr_{0.2}Sr_{0.2})Co_{1.5}Fe_{0.5}O_{6-d}$) was developed by Dr Kim during his PhD and the work is published and referenced.[22]

The SI file includes additional images and micrographs of the tubes (bisque-fired, dip-coated before and after sintering). Nyquist plots and DRT collected upon electrolysis testing are also provided. See DOI: https://doi.org/10.1039/d6ma00171h.

Acknowledgements

This work was supported by the U.S. Department of Energy under Award No. DE-EE0011337: Advanced Materials and Operating Conditions for Intermediate-Temperature Protonic-Ceramic Steam Electrolysis (P-SOEC). The authors would also like to acknowledge Dr Yewon Shin for her help in the sample reduction (Fig. 2 and 3). HyET NoCarbon would like to thank

NWO and GroenvermogenNL for supporting this work under the HyPRO (GVNL WP1) project.

Notes and references

1 L. Lei, J. Zhang, Z. Yuan, J. Liu, M. Ni and F. Chen, *Adv. Funct. Mater.*, 2019, **29**, 1903805.
2 D. Medvedev, *Int. J. Hydrogen Energy*, 2019, **44**, 26711–26740.
3 K. Leonard, W. Deibert, M. E. Ivanova, W. A. Meulenberg, T. Ishihara and H. Matsumoto, *Membranes*, 2020, **10**, 339.
4 C. Duan, R. Kee, H. Zhu, N. Sullivan, L. Zhu, L. Bian, D. Jennings and R. O'Hayre, *Nat. Energy*, 2019, **4**, 230–240.
5 E. D. Wachsman and K. T. Lee, *Science*, 2011, **334**, 935–939.
6 C. Meisel, J. D. Huang, L. Q. Le, Y.-D. Kim, S. Stockburger, Z. Luo, T. Zhu, Z. Wang, Z. Shao, R. O'Hayre and N. P. Sullivan, *J. Mater. Chem. A*, 2025, **13**, 10863–10880.
7 L. Q. Le, C. Meisel, C. H. Hernandez, J. Huang, Y. Kim, R. O'Hayre and N. P. Sullivan, *J. Power Sources*, 2022, **537**, 231356.
8 Y.-D. Kim, C. Meisel, I.-H. Kim, C. Herradón, P. Rand, J. Yang, N. P. Sullivan and R. O'Hayre, *J. Power Sources*, 2025, **625**, 235700.
9 Y. Kim, I. Kim, C. Meisel, C. Herradón, P. Rand, J. Yang, H. S. Kim, N. Sullivan and R. O'Hayre, *J. Phys.: Energy*, 2024, **6**, 035004.
10 C. Ren, S. Wang, T. Liu, Y. Lin and F. Chen, *J. Power Sources*, 2015, **290**, 1–7.
11 S. Ricote, R. J. Kee and W. G. Coors, *Membranes*, 2022, **12**, 242.
12 A. R. Hanifi, S. Paulson, A. Torabi, A. Shinbine, M. C. Tucker, V. Birss, T. H. Etsell and P. Sarkar, *J. Power Sources*, 2014, **266**, 121–131.
13 L. Zhang, H. Q. He, W. R. Kwek, J. Ma, E. H. Tang and S. P. Jiang, *J. Am. Ceram. Soc.*, 2009, **92**, 302–310.
14 Z. Chen and L. Turng, *Adv. Polym. Technol.*, 2005, **24**, 165–182.
15 C. Fernandes, A. J. Pontes, J. C. Viana and A. Gaspar-Cunha, *Adv. Polym. Technol.*, 2018, **37**, 429–449.
16 J. Wang, *Some critical issues for injection molding*, BoD–Books on Demand, 2012.
17 T. Jardiel, M. E. Sotomayor, B. Levenfeld and A. Várez, *Int. J. Appl. Ceram. Technol.*, 2008, **5**, 574–581.
18 A. Faes, H. Girard, A. Zryd and Z. Wuillemin, *J. Power Sources*, 2013, **227**, 35–40.
19 J. Xiao, X. Zeng, M. Li, P. Dong, H. Wu, M. Xu, Y. Lin, J. Liu, Y. Xie and Y. Zhang, *Ceram. Int.*, 2019, **45**, 20066–20072.
20 J. Xiao, W. Cai, J. Liu and M. Liu, *Int. J. Hydrogen Energy*, 2014, **39**, 5105–5112.
21 J. Kupecki, R. Kluczowski, D. Papurello, A. Lanzini, M. Kawalec, M. Krauz and M. Santarelli, *Int. J. Hydrogen Energy*, 2019, **44**, 19405–19411.
22 Y. Kim, P. Rand, E. Brim, C. Meisel, S. R. Goldy, J. Yang, M. Sanders, H. S. Kim, K. Jo, H. Lee, G. J. Tucker, C. V. Ciobanu, R. M. Richards, N. P. Sullivan and R. O'Hayre, *Appl. Catal., B: Environ. Energy*, 2025, **378**, 125590.
23 H. Su and Y. H. Hu, *Energy Sci. Eng.*, 2022, **10**(5), 1706–1725.